

Joint DNN-Based Multichannel Reduction of Acoustic Echo, Reverberation and Noise

Guillaume Carbajal, *Student Member, IEEE*, Romain Serizel, *Member, IEEE*, Emmanuel Vincent, *Senior Member, IEEE*, and Eric Humbert, *Member, IEEE*

Abstract—We consider the problem of simultaneous reduction of acoustic echo, reverberation and noise. In real scenarios, these distortion sources may occur simultaneously and reducing them implies combining the corresponding distortion-specific filters. As these filters interact with each other, they must be jointly optimized. We propose to model the target and residual signals after linear echo cancellation and dereverberation using a multichannel Gaussian modeling framework and to jointly represent their spectra by means of a neural network. We develop an iterative block-coordinate ascent algorithm to update all the filters. We evaluate our system on real recordings of acoustic echo, reverberation and noise acquired with a smart speaker in various situations. The proposed approach outperforms in terms of overall distortion a cascade of the individual approaches and a joint reduction approach which does not rely on a spectral model of the target and residual signals.

Index Terms—Acoustic echo, reverberation, background noise, joint distortion reduction, expectation-maximization, recurrent neural network.

I. INTRODUCTION

IN hands-free telecommunications, a speaker from a near-end point interacts with another speaker at a far-end point. The near-end speaker can be a few meters away from the microphones and the interactions can be subject to several distortion sources such as background noise, acoustic echo and near-end reverberation. Each of these distortion sources degrades speech quality, intelligibility and listening comfort, and must be reduced.

Single- and multichannel filters have been used to reduce each of these distortion sources independently. They can be categorized into short nonlinear filters that vary quickly over time and long linear filters that are time-invariant (or slowly time-varying). Short nonlinear filters are generally used for noise reduction [1]. They are robust to the fluctuations and nonlinearities inherent to real signals. Long linear filters can be required for dereverberation [2] and echo reduction [3]. They are able to reduce most of the distortion sources in time-invariant conditions without introducing any artifact, or musical noise, in the near-end signal.

When several distortion sources occur simultaneously, reducing them requires cascading the distortion-specific filters. However, as these filters interact with each other, tuning them independently can be suboptimal and even lead to additional

distortions. Several joint approaches that handle two distortion sources have been proposed, namely for joint dereverberation and source separation/noise reduction [4]–[9], for joint echo and noise reduction [10]–[15], and for joint echo reduction and dereverberation [16], [17].

A joint approach for single-channel echo reduction, dereverberation and noise reduction was proposed by Habets et al. [18]. However, the linear echo cancellation filter was ignored in the optimization process. To the best of our knowledge, only Togami et al. proposed a solution optimizing two linear filters and a nonlinear postfilter for reducing echo, reverberation and noise [19]. They represented the filter interactions by modeling the target and residual signals after echo cancellation and dereverberation within a multichannel Gaussian framework. However, no model was proposed for the short term spectra of these signals. This results in misestimation of the linear filters and the nonlinear postfilter.

Recently, deep neural networks (DNN) have shown promising results to estimate the short term spectra of speech and distortion sources for joint dereverberation and source separation/noise reduction [20], [21], and for joint echo and noise reduction [22], [23]. However, these DNN-based approaches have only focused on reducing two distortion sources.

In this article, we propose a DNN-based approach for joint multichannel reduction of echo, reverberation and noise. We simultaneously model the spatial and spectral parameters of the target and residual signals within a multichannel Gaussian framework and we derive an iterative a block-coordinate ascent (BCA) algorithm to update the echo cancellation, dereverberation and noise/residual reduction filters. We evaluate our system on real recordings of acoustic echo, near-end reverberation and background noise acquired with a smart speaker in various situations. We experimentally show the effectiveness of our proposed approach compared with a cascade of individual approaches and Togami et al.’s joint reduction approach [19].

The rest of this article is organized as follows. In Section II, we describe existing enhancement methods designed for the separate reduction of echo, reverberation or noise, and Togami et al.’s approach. We explain our joint approach using a DNN spectral model within a BCA algorithm in Section III. In Section IV we detail our DNN-based joint spectral model. Section V describes the experimental settings for the training and evaluation of our approach. Section VI shows the results of our approach compared to the cascade of individual approaches and Togami et al.’s approach. Finally Section VII concludes the article and provides future directions.

M. Carbajal and E. Humbert are with Invoxia SAS, 2 Rue Maurice Hartmann, 92130 Issy-les-Moulineaux, France (email: guillaume.carbajal@invoxia.com, eric.humbert@invoxia.com). R. Serizel and E. Vincent are with Université de Lorraine, CNRS, Inria, LORIA, F-54000 Nancy, France (email: romain.serizel@loria.fr, emmanuel.vincent@inria.fr).

II. BACKGROUND

In this section, we first describe multichannel approaches for the separate reduction of echo, reverberation or noise. These approaches will be used as building blocks for our solution and a basis for comparison in our experiments. We then describe Togami et al.'s joint approach. We adopt the following notations through the article: scalars are represented by plain letters, vectors by bold lowercase letters, and matrices by bold uppercase letters. The symbol $(\cdot)^*$ refers to complex conjugation, $(\cdot)^T$ to matrix transposition, $(\cdot)^H$ to Hermitian transposition, $\text{tr}(\cdot)$ to the trace of a matrix, $\|\cdot\|$ to the Euclidean norm and \otimes to the Kronecker product. The identity matrix is denoted as \mathbf{I} . Its dimension is either implied by the context or explicitly specified by a subscript.

A. Echo reduction

The echo reduction problem is defined as follows. Denoting by M the number of channels (microphones), the mixture $\mathbf{d}^{\text{echo}}(t) \in \mathbb{R}^{M \times 1}$ observed at the microphones at time t is the sum of the near-end signal $\mathbf{s}(t) \in \mathbb{R}^{M \times 1}$ and the acoustic echo $\mathbf{y}(t) \in \mathbb{R}^{M \times 1}$:

$$\mathbf{d}^{\text{echo}}(t) = \mathbf{s}(t) + \mathbf{y}(t). \quad (1)$$

The acoustic echo $\mathbf{y}(t)$ is a nonlinearly distorted version of the observed far-end signal $x(t) \in \mathbb{R}$ played by the loudspeaker, which is assumed to be single-channel. The linear part can be approximated by the linear convolution of $x(t)$ and the M -dimensional room impulse response (RIR) $\mathbf{a}_y(\tau) \in \mathbb{R}^{M \times 1}$, or echo path, modeling the acoustic path from the loudspeaker (including the loudspeaker response) to the microphones. The echo signal can be expressed as

$$\mathbf{y}(t) \approx \sum_{\tau=0}^{\infty} \mathbf{a}_y(\tau)x(t-\tau). \quad (2)$$

The signals are transformed into the time-frequency domain by the short-time Fourier transform (STFT)

$$\mathbf{d}^{\text{echo}}(n, f) = \mathbf{s}(n, f) + \mathbf{y}(n, f), \quad (3)$$

at time frame index $n \in [0, N-1]$ and frequency bin index $f \in [0, F-1]$, where F is the number of frequency bins and N the number of time frames of the utterance. As the far-end signal $x(n, f) \in \mathbb{C}$ is known, the goal is to recover the M -dimensional near-end speech $\mathbf{s}(n, f) \in \mathbb{C}^{M \times 1}$ from the mixture $\mathbf{d}^{\text{echo}}(n, f) \in \mathbb{C}^{M \times 1}$ by identifying the echo path $\{\mathbf{a}_y(n, f)\}_{n,f}$. The underlying idea is to estimate $\mathbf{y}(n, f) \in \mathbb{C}^{M \times 1}$ with a long, multiframe linear echo cancellation filter $\underline{\mathbf{H}}(f) = [\mathbf{h}(0, f) \dots \mathbf{h}(K-1, f)] \in \mathbb{C}^{M \times K}$ applied on the K previous frames of the far-end signal $x(n, f)$, and to subtract the resulting signal $\hat{\mathbf{y}}(n, f)$ from $\mathbf{d}^{\text{echo}}(n, f)$:

$$\mathbf{e}^{\text{echo}}(n, f) = \mathbf{d}^{\text{echo}}(n, f) - \underbrace{\sum_{k=0}^{K-1} \mathbf{h}(k, f)x(n-k, f)}_{=\hat{\mathbf{y}}(n, f)}. \quad (4)$$

where $\mathbf{h}(k, f) \in \mathbb{C}^{M \times 1}$ is the M -dimensional vector corresponding to the k -th tap of $\underline{\mathbf{H}}(f)$. Note that the tap k is measured in frames and the underscore notation in $\underline{\mathbf{H}}(f)$ denotes

the concatenation of the K taps of $\mathbf{h}(k, f)$. Since the far-end signal $x(n, f)$ is known, the filter $\underline{\mathbf{H}}(f)$ is usually estimated adaptively in the minimum mean square error (MMSE) sense [3]. Adaptive MMSE optimization typically relies on adaptive algorithms such as least mean squares (LMS) which adjust the filter $\underline{\mathbf{H}}(f)$ in an online manner by stochastic gradient descent with a time-varying step size [3]. These algorithms have low complexity and fast convergence, which makes them particularly suitable for time-varying conditions. Yang et al. provide a comprehensive review of optimal step size selection for echo reduction [24].

In practice, the output signal $\mathbf{e}^{\text{echo}}(n, f)$ is not equal to the near-end speech $\mathbf{s}(n, f)$, not only because of the estimation error, but also because of the smaller length of $\underline{\mathbf{H}}(f)$ compared to the true echo path and of nonlinearities that cannot be modeled by $\underline{\mathbf{H}}(f)$ [18]. As a result, a residual echo $\mathbf{z}(n, f)$ remains that can be expressed as [3]

$$\mathbf{e}^{\text{echo}}(n, f) - \mathbf{s}(n, f) = \underbrace{\mathbf{y}(n, f) - \hat{\mathbf{y}}(n, f)}_{=\mathbf{z}(n, f)}. \quad (5)$$

To overcome this limitation, a (nonlinear) residual echo suppression postfilter $\mathbf{W}^{\text{echo}}(n, f) \in \mathbb{C}^{M \times M}$ is typically applied:

$$\hat{\mathbf{s}}(n, f) = \mathbf{W}^{\text{echo}}(n, f)\mathbf{e}^{\text{echo}}(n, f). \quad (6)$$

There exist multiple approaches to derive $\mathbf{W}^{\text{echo}}(n, f)$ [3]. Recently, direct estimation of $\mathbf{W}^{\text{echo}}(n, f)$ using a DNN has shown good performance in the single-channel case [25], [26]. However, when $\underline{\mathbf{H}}(f)$ changes, $\mathbf{z}(n, f)$ also changes and the postfilter $\mathbf{W}^{\text{echo}}(n, f)$ must be adapted consequently. Estimating $\underline{\mathbf{H}}(f)$ and $\mathbf{W}^{\text{echo}}(n, f)$ separately is thus suboptimal. Joint optimization of $\underline{\mathbf{H}}(f)$ and $\mathbf{W}^{\text{echo}}(n, f)$ was investigated in the MMSE and the maximum likelihood (ML) sense [27], [28].

In Section V, we will use adaptive MMSE optimization for estimating the echo cancellation filter $\underline{\mathbf{H}}(f)$ as a part of the cascade of the individual approaches to which we compare our joint approach.

B. Near-end dereverberation

The near-end dereverberation problem is defined as follows. The signal $\mathbf{d}^{\text{rev}}(t)$ observed at the microphones at time t is just the reverberant near-end signal $\mathbf{s}(t)$, which is obtained by linear convolution of the anechoic near-end signal $u(t) \in \mathbb{R}$ and the M -dimensional RIR $\mathbf{a}_s(\tau) \in \mathbb{R}^{M \times 1}$:

$$\mathbf{d}^{\text{rev}}(t) = \mathbf{s}(t) = \sum_{\tau=0}^{\infty} \mathbf{a}_s(\tau)u(t-\tau). \quad (7)$$

This signal can be decomposed as

$$\mathbf{s}(t) = \underbrace{\sum_{0 \leq \tau \leq t_e} \mathbf{a}_s(\tau)u(t-\tau)}_{=\mathbf{s}_e(t)} + \underbrace{\sum_{\tau > t_e} \mathbf{a}_s(\tau)u(t-\tau)}_{=\mathbf{s}_l(t)}, \quad (8)$$

where $\mathbf{s}_e(t)$ denotes the early near-end signal component, $\mathbf{s}_l(t)$ the late reverberation component, and t_e is the mixing time. The component $\mathbf{s}_e(t)$ comprises the main peak of the RIR (the direct path) and the early reflections within a delay t_e which contribute to speech quality and intelligibility. The component

$s_1(t)$ comprises all the later reflections which degrade intelligibility. In the time-frequency domain, the reverberant near-end speech can thus be expressed as

$$s(n, f) = s_e(n, f) + s_1(n, f). \quad (9)$$

The goal is to recover the early near-end component $s_e(n, f)$ from the reverberant near-end signal $s(n, f)$. Naylor et al. provided a comprehensive review of dereverberation approaches [2]. Among them, the weighted prediction error (WPE) method [29] estimates $s_1(n, f)$ by inverse filtering with a long, multi-frame linear filter $\underline{\mathbf{G}}(f) = [\mathbf{G}(\Delta, f) \dots \mathbf{G}(\Delta + L - 1, f)] \in \mathbb{C}^{M \times ML}$ applied on the L previous frames of the mixture signal $s(n - \Delta, f)$ defined in (7). The delay Δ is introduced to avoid over-whitening of the near-end speech. The resulting signal $\widehat{s}_1(n, f)$ is then subtracted from the mixture signal $s(n, f)$ defined in (7):

$$\mathbf{r}^{\text{rev}}(n, f) = s(n, f) - \underbrace{\sum_{l=\Delta}^{\Delta+L-1} \mathbf{G}(l, f) s(n-l, f)}_{\widehat{s}_1(n, f)}. \quad (10)$$

where $\mathbf{G}(l, f) = [\mathbf{g}_1(l, f) \dots \mathbf{g}_M(l, f)] \in \mathbb{C}^{M \times M}$ is the $M \times M$ -dimensional matrix corresponding to the l -th tap of $\underline{\mathbf{G}}(f)$. As the component $s_e(n, f)$ is not an observed signal, Nakatani et al. estimated the filter $\underline{\mathbf{G}}(f)$ in the ML sense by modeling $s_e(n, f)$ as a directional source [29]. However, they did not impose any constraint on its short-term spectrum which results in limited dereverberation [29], [30]. Other authors have assumed a model of the short-term spectrum. Yoshioka et al. used an all-pole model [8], Kagami et al. used nonnegative matrix factorization (NMF) [9], Jukić et al. used sparse priors [31], and Kinoshita et al. used a DNN [32].

For several reasons, including the smaller length of the filter compared to true near-end RIR and potentially time-varying conditions, a residual late reverberation component $s_r(n, f)$ remains [33]–[35] that can be expressed as

$$\mathbf{r}^{\text{rev}}(n, f) - s_e(n, f) = \underbrace{s_1(n, f) - \widehat{s}_1(n, f)}_{=s_r(n, f)}. \quad (11)$$

To overcome this limitation, a (nonlinear) residual reverberation suppression postfilter $\mathbf{W}^{\text{rev}}(n, f) \in \mathbb{C}^{M \times M}$ is applied on the signal $\mathbf{r}^{\text{rev}}(n, f)$:

$$\widehat{s}_e(n, f) = \mathbf{W}^{\text{rev}}(n, f) \mathbf{r}^{\text{rev}}(n, f). \quad (12)$$

There are multiple approaches to derive $\mathbf{W}^{\text{rev}}(n, f)$ [33], [35]. However, when $\underline{\mathbf{G}}(f)$ changes, $s_r(n, f)$ also changes and the postfilter $\mathbf{W}^{\text{rev}}(n, f)$ must be adapted consequently. Estimating $\underline{\mathbf{G}}(f)$ and $\mathbf{W}^{\text{rev}}(n, f)$ separately is thus suboptimal. Joint optimization of $\underline{\mathbf{G}}(f)$ and $\mathbf{W}^{\text{rev}}(n, f)$ was investigated in the ML sense [34].

In section V, we will use WPE for estimating the dereverberation filter $\underline{\mathbf{G}}(f)$ as a part of the cascade of the individual approaches to which we compare our joint approach.

C. Noise reduction

The noise reduction problem is defined as follows. In the time-frequency domain, the M -channel mixture $\mathbf{d}^{\text{noise}}(n, f)$

observed at the microphones is the sum of the near-end signal $s(n, f)$ and a noise signal $\mathbf{b}(n, f) \in \mathbb{C}^{M \times 1}$:

$$\mathbf{d}^{\text{noise}}(n, f) = \mathbf{s}(n, f) + \mathbf{b}(n, f). \quad (13)$$

Note that the noise signal $\mathbf{b}(n, f)$ can be either spatially diffuse or localized. The goal is to recover the near-end speech $s(n, f)$ from the mixture $\mathbf{d}^{\text{noise}}(n, f)$. This is typically achieved by applying a short nonlinear filter $\mathbf{W}_s^{\text{noise}}(n, f) \in \mathbb{C}^{M \times M}$ on $\mathbf{d}^{\text{noise}}(n, f)$:

$$\widehat{\mathbf{s}}(n, f) = \mathbf{W}^{\text{noise}}(n, f) \mathbf{d}^{\text{noise}}(n, f). \quad (14)$$

The filter can be estimated in the MMSE or ML sense. Gannot et al. provide a comprehensive review of spatial filtering solutions [36]. One family of solutions relies on multichannel time-varying Wiener filtering, where the filter is derived from a local Gaussian model of the target and noise sources [37]. The spectral parameters (short term power spectra) and the spatial parameters (spatial covariance matrices) of this model are estimated in the ML sense. Since there is no closed form solution, the ML parameters are estimated using an EM algorithm. When no constraint is imposed on the spectral or spatial parameters, the EM algorithm operates in each frequency bin f independently which results in a permutation ambiguity in the separated components at each frequency bin f and requires additional permutation alignment. Alternatively, the spectral parameters can be estimated with a model. Ozerov et al. used NMF [38], Nugraha et al. used a DNN [39], and recently variational autoencoders were used [40].

In Section V, we will use multichannel time-varying Wiener filtering as a part of the cascade of the individual approaches to which we compare our joint approach.

D. Joint reduction of echo, reverberation and noise

In real scenarios, all the distortions introduced above can be simultaneously present as illustrated in Fig. 1. The mixture $\mathbf{d}(n, f)$ observed at the microphones is thus the sum of the acoustic echo $\mathbf{y}(n, f)$, the reverberant near-end signal $s(n, f)$ and the noise $\mathbf{b}(n, f)$

$$\mathbf{d}(n, f) = \mathbf{s}(n, f) + \mathbf{y}(n, f) + \mathbf{b}(n, f) \quad (15)$$

$$= s_e(n, f) + s_1(n, f) + \mathbf{y}(n, f) + \mathbf{b}(n, f). \quad (16)$$

The goal is to recover the early near-end component $s_e(n, f)$ from the mixture $\mathbf{d}(n, f)$.

Togami et al. proposed a joint approach combining an echo cancellation filter $\underline{\mathbf{H}}(f)$ (see Section II-A), a dereverberation

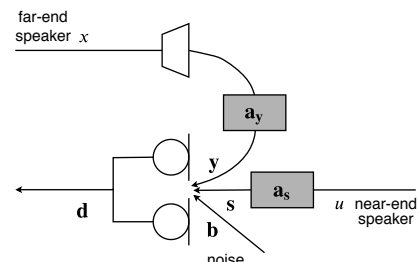


Fig. 1: Acoustic echo, reverberation and noise problem.

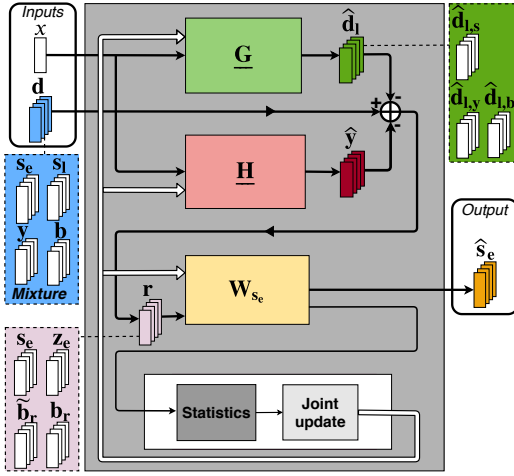


Fig. 2: Togami et al.'s approach for joint reduction of echo, reverb, and noise [19]. The bold arrows denote the filtering steps. The dashed lines denote the latent signal components. The thin arrows denote the signals used for the joint update. The white arrows denote the filter updates.

filter $\underline{\mathbf{G}}(f)$ (see Section II-B), and a nonlinear multichannel Wiener postfilter $\mathbf{W}_{s_e}(n, f)$ (see Section II-C) [19]. The approach is illustrated in Fig. 2. In the first step, they apply the echo cancellation filter $\underline{\mathbf{H}}(f)$ as in (4) and subtract the resulting echo estimate $\hat{\mathbf{y}}(n, f)$ from the mixture signal $\mathbf{d}(n, f)$. In parallel, the authors apply the dereverberation filter $\underline{\mathbf{G}}(f)$ on the mixture signal $\mathbf{d}(n, f)$ as in (10) and subtract the resulting late reverberation estimate $\hat{\mathbf{d}}_l(n, f)$ from $\mathbf{d}(n, f)$. The resulting signal $\mathbf{r}(n, f)$ after echo cancellation and dereverberation is then

$$\mathbf{r}(n, f) = \mathbf{d}(n, f) - \hat{\mathbf{y}}(n, f) - \underbrace{\sum_{l=\Delta}^{\Delta+L-1} \mathbf{G}(l, f) \mathbf{d}(n-l, f)}_{=\hat{\mathbf{d}}_l(n, f)}. \quad (17)$$

Due to the reasons mentioned in Sections II-A and II-B, and to the presence of the noise signal $\mathbf{b}(n, f)$, undesired residual signals remain and can be expressed as

$$\mathbf{r}(n, f) - \mathbf{s}_e(n, f) = \mathbf{z}_e(n, f) + \tilde{\mathbf{b}}_r(n, f) + \mathbf{b}_r(n, f). \quad (18)$$

The signals $\mathbf{z}_e(n, f)$, $\tilde{\mathbf{b}}_r(n, f)$ and $\mathbf{b}_r(n, f)$ are defined as

$$\mathbf{z}_e(n, f) = \mathbf{y}_e(n, f) - \hat{\mathbf{y}}(n, f), \quad (19)$$

$$\tilde{\mathbf{b}}_r(n, f) = \mathbf{s}_1(n, f) - \hat{\mathbf{d}}_{l,s}(n, f) + \mathbf{y}_1(n, f) - \hat{\mathbf{d}}_{l,y}(n, f), \quad (20)$$

$$\mathbf{b}_r(n, f) = \mathbf{b}(n, f) - \hat{\mathbf{d}}_{l,b}(n, f), \quad (21)$$

where the signals $\mathbf{y}_e(n, f)$ and $\mathbf{y}_1(n, f)$ denote the early component and the late reverberation of the echo $\mathbf{y}(n, f)$, respectively, $\hat{\mathbf{d}}_{l,s}(n, f) = \sum_{l=\Delta}^{\Delta+L-1} \mathbf{G}(l, f) \mathbf{s}(n-l, f)$, $\hat{\mathbf{d}}_{l,y}(n, f) = \sum_{l=\Delta}^{\Delta+L-1} \mathbf{G}(l, f) \mathbf{y}(n-l, f)$ and $\hat{\mathbf{d}}_{l,b}(n, f) = \sum_{l=\Delta}^{\Delta+L-1} \mathbf{G}(l, f) \mathbf{b}(n-l, f)$ are the latent components of $\hat{\mathbf{d}}_l(n, f)$ resulting from (17), and $\mathbf{b}_r(n, f)$ is the *dereverberated* noise signal. The term *dereverberated* means "after applying the dereverberation filter".

To recover the early near-end signal component $\mathbf{s}_e(n, f)$ from the signal $\mathbf{r}(n, f)$, the authors applied a multichannel Wiener postfilter $\mathbf{W}_{s_e}(n, f) \in \mathbb{C}^{M \times M}$ on the signal $\mathbf{r}(n, f)$:

$$\hat{\mathbf{s}}_e(n, f) = \mathbf{W}_{s_e}(n, f) \mathbf{r}(n, f). \quad (22)$$

The authors estimated $\underline{\mathbf{H}}(f)$, $\underline{\mathbf{G}}(f)$ and $\mathbf{W}_{s_e}(n, f)$ by modeling $\mathbf{s}_e(n, f)$ and $\mathbf{b}_r(n, f)$ as zero-mean multichannel Gaussian variables, and $\mathbf{z}_e(n, f)$ and $\tilde{\mathbf{b}}_r(n, f)$ as nonzero-mean multichannel Gaussian variables [19]. They used an EM algorithm to jointly optimize the spectral and spatial parameters of this model in the ML sense.

However, their approach suffers from several limitations. First, they did not impose any constraint on the spectral parameters of the target $\mathbf{s}_e(n, f)$ and the *dereverberated* noise signal $\mathbf{b}_r(n, f)$. Secondly, the signal components $\mathbf{s}_1(n, f)$ and $\mathbf{y}_1(n, f)$ in $\mathbf{b}_r(n, f)$ are not separately modeled, i.e. these components share the same spatial parameters, which is not the case in practice. These two limitations result in misestimation of the filters $\underline{\mathbf{H}}(f)$, $\underline{\mathbf{G}}(f)$ and the postfilter $\mathbf{W}_{s_e}(n, f)$. Thirdly, because the filters $\underline{\mathbf{H}}(f)$ and $\underline{\mathbf{G}}(f)$ operate independently on the mixture signal $\mathbf{d}(n, f)$, their respective components $\hat{\mathbf{y}}(n, f)$ and $\hat{\mathbf{d}}_{l,y}(n, f)$ subtracted from the echo $\mathbf{y}(n, f)$ in (19) and (20) might interfere with each other. Finally, since the echo $\mathbf{y}(n, f)$ is often much louder than the near-end speech $\mathbf{s}(n, f)$ and the noise signal $\mathbf{b}(n, f)$ in $\mathbf{d}(n, f)$, the dereverberation filter $\underline{\mathbf{G}}(f)$ here mainly reduces the late reverberation of the echo $\mathbf{y}_1(n, f)$ instead of the reverberation of the near-end speech $\mathbf{s}_1(n, f)$.

III. DNN-BASED BCA ALGORITHM FOR JOINT REDUCTION OF ECHO, REVERBERATION AND NOISE

In this section, we propose a joint DNN-based model to estimate the spectral parameters of the target and the residual signals. We derive a DNN-based BCA algorithm for joint reduction of echo, reverberation and noise that exploits these estimated spectral parameters for an accurate derivation of the echo cancellation and dereverberation filters and the nonlinear postfilter.

A. Model

The approach is illustrated in Fig. 3. In the first step, we apply the echo cancellation filter $\underline{\mathbf{H}}(f)$ as in (4) and subtract the resulting echo estimate $\hat{\mathbf{y}}(n, f)$ from $\mathbf{d}(n, f)$:

$$\mathbf{e}(n, f) = \mathbf{d}(n, f) - \underbrace{\sum_{k=0}^{K-1} \mathbf{h}(k, f) x(n-k, f)}_{=\hat{\mathbf{y}}(n, f)}. \quad (23)$$

The resulting signal $\mathbf{e}(n, f)$ contains the near-end signal $\mathbf{s}(n, f)$, the residual echo $\mathbf{z}(n, f)$ and the noise signal $\mathbf{b}(n, f)$. Unlike Togami et al. [19], we do not apply the dereverberation filter $\underline{\mathbf{G}}(f)$ on the mixture signal $\mathbf{d}(n, f)$, but on the signal $\mathbf{e}(n, f)$ and subtract the resulting late reverberation estimate $\hat{\mathbf{e}}_l(n, f)$ from $\mathbf{e}(n, f)$. To the best of our knowledge, this is the first work where the dereverberation filter $\underline{\mathbf{G}}(f)$ is applied after the echo cancellation filter $\underline{\mathbf{H}}(f)$ in the context of joint echo reduction of echo, reverberation

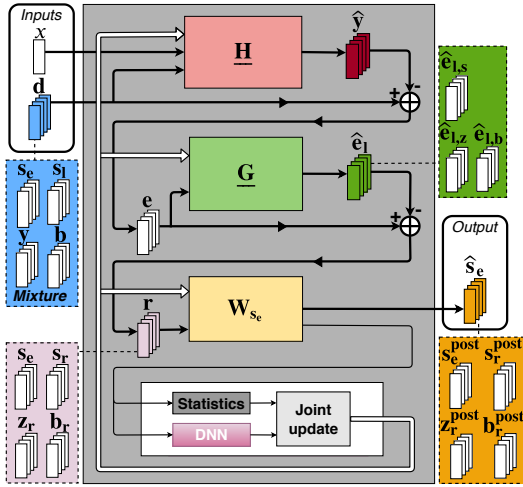


Fig. 3: Proposed approach. Arrows and lines have the same meaning as in Fig. 2.

and noise. The resulting signal $\mathbf{r}(n, f)$ is thus expressed as

$$\mathbf{r}(n, f) = \mathbf{e}(n, f) - \underbrace{\sum_{l=\Delta}^{\Delta+L-1} \mathbf{G}(l, f)\mathbf{e}(n-l, f)}_{=\hat{\mathbf{e}}_1(n, f)}. \quad (24)$$

Since the linear filters $\mathbf{H}(f)$ and $\mathbf{G}(f)$ are causal, we make the assumption that the observed signals $\mathbf{d}(n, f)$ and $x(n, f)$ are equal to zero for $n < 0$. Since the residual echo $\mathbf{z}(n, f)$ in $\mathbf{e}(n, f)$ is a reduced version of the echo $\mathbf{y}(n, f)$ in $\mathbf{d}(n, f)$, the dereverberation filter $\mathbf{G}(f)$ achieves a greater reduction of the near-end late reverberation $\mathbf{s}_1(n, f)$ than in Togami et al.'s approach [19]. Due to the reasons mentioned in Sections II-A and II-B, and to the presence of the noise signal $\mathbf{b}(n, f)$, undesired residual signals remain and can be expressed as

$$\mathbf{r}(n, f) - \mathbf{s}_c(n, f) = \mathbf{s}_r(n, f) + \mathbf{z}_r(n, f) + \mathbf{b}_r(n, f), \quad (25)$$

where $\mathbf{s}_r(n, f)$ is the residual late reverberation near-end component, $\mathbf{z}_r(n, f)$ the *dereverberated* residual echo, and $\mathbf{b}_r(n, f)$ the *dereverberated* noise. The signal $\mathbf{s}_r(n, f)$, $\mathbf{z}_r(n, f)$ and $\mathbf{b}_r(n, f)$ are defined as

$$\mathbf{s}_r(n, f) = \mathbf{s}_1(n, f) - \hat{\mathbf{e}}_{1,s}(n, f), \quad (26)$$

$$\mathbf{z}_r(n, f) = \mathbf{z}(n, f) - \hat{\mathbf{e}}_{1,z}(n, f), \quad (27)$$

$$\mathbf{b}_r(n, f) = \mathbf{b}(n, f) - \hat{\mathbf{e}}_{1,b}(n, f), \quad (28)$$

where the signals $\hat{\mathbf{e}}_{1,s}(n, f) = \sum_{l=\Delta}^{\Delta+L-1} \mathbf{G}(l, f)\mathbf{s}(n-l, f)$, $\hat{\mathbf{e}}_{1,z}(n, f) = \sum_{l=\Delta}^{\Delta+L-1} \mathbf{G}(l, f)\mathbf{z}(n-l, f)$ and $\hat{\mathbf{e}}_{1,b}(n, f) = \sum_{l=\Delta}^{\Delta+L-1} \mathbf{G}(l, f)\mathbf{b}(n-l, f)$ are the latent components of $\hat{\mathbf{e}}_1(n, f)$ resulting from (24). To recover the signal $\mathbf{s}_c(n, f)$ from the signal $\mathbf{r}(n, f)$, we apply a multichannel Wiener postfilter $\mathbf{W}_{s_c}(n, f) \in \mathbb{C}^{M \times M}$ on the signal $\mathbf{r}(n, f)$ as

$$\hat{\mathbf{s}}_c(n, f) = \mathbf{W}_{s_c}(n, f)\mathbf{r}(n, f). \quad (29)$$

Inspired by WPE for dereverberation [29], we estimate $\mathbf{H}(f)$, $\mathbf{G}(f)$ and $\mathbf{W}_{s_c}(n, f)$ by modeling the target $\mathbf{s}_c(n, f)$ and the three residual signals $\mathbf{s}_r(n, f)$, $\mathbf{z}_r(n, f)$ and $\mathbf{b}_r(n, f)$ with a multichannel local Gaussian framework. In the fol-

lowing we use the general notation $\mathbf{c}(n, f)$ to denote each one of these four signals, and consider them as *sources* to be separated. Each of these four sources is modeled as

$$\mathbf{c}(n, f) \sim \mathcal{N}(\mathbf{0}, v_c(n, f)\mathbf{R}_c(f)), \quad (30)$$

where $v_c(n, f) \in \mathbb{R}_+$ and $\mathbf{R}_c(f) \in \mathbb{C}^{M \times M}$ denote the power spectral density (PSD) and the spatial covariance matrix (SCM) of the source, respectively [37]. The multichannel Wiener filter for the source $\mathbf{c}(n, f)$ is formulated as

$$\mathbf{W}_c(n, f) = v_c(n, f)\mathbf{R}_c(f) \left(\sum_{c'} v_{c'}(n, f)\mathbf{R}_{c'}(f) \right)^{-1}, \quad (31)$$

where the sum over c' includes all four sources. The postfilter $\mathbf{W}_{s_c}(n, f)$ is a specific case of (31) where $\mathbf{c}(n, f) = \mathbf{s}_c(n, f)$.

B. Likelihood

In order to estimate the parameters of this model, we must first express its likelihood. Following (23), (24), (25) and (30), the log-likelihood of the observed sequence $\mathcal{O} = \{\mathbf{d}(n, f), x(n, f)\}_{n,f}$ is given by

$$\begin{aligned} \mathcal{L}(\mathcal{O}; \Theta_H, \Theta_G, \Theta_c) &= \sum_{f=0}^{F-1} \sum_{n=0}^{N-1} \log p(\mathbf{d}(n, f) | \mathbf{d}(n-1, f), \dots, \mathbf{d}(0, f), \\ &\quad x(n, f), \dots, x(0, f)), \\ &= \sum_{f=0}^{F-1} \sum_{n=0}^{N-1} \log \mathcal{N}_{\mathbb{C}}(\mathbf{d}(n, f); \boldsymbol{\mu}_d(n, f), \mathbf{R}_{dd}(n, f)), \end{aligned} \quad (32)$$

where

$$\begin{aligned} \boldsymbol{\mu}_d(n, f) &= \sum_{k=0}^{K-1} \mathbf{h}(k, f)x(n-k, f) \\ &\quad + \sum_{l=\Delta}^{\Delta+L-1} \mathbf{G}(l, f)\mathbf{e}(n-l, f), \end{aligned} \quad (34)$$

$$\mathbf{R}_{dd}(n, f) = \sum_{c'} v_{c'}(n, f)\mathbf{R}_{c'}(f), \quad (35)$$

and $\Theta_H = \{\mathbf{H}(f)\}_f$, $\Theta_G = \{\mathbf{G}(f)\}_f$ and $\Theta_c = \{v_c(n, f), \mathbf{R}_c(f)\}_{c,n,f}$ are the parameters to be estimated. The resulting ML optimization problem has no closed form solution, hence we need to estimate the parameters via an iterative procedure.

C. Iterative optimization algorithm

We propose a BCA algorithm for likelihood optimization. Each iteration i comprises the following three maximization steps:

$$\hat{\Theta}_H \leftarrow \underset{\Theta_H}{\operatorname{argmax}} \mathcal{L}(\mathcal{D}; \Theta_H, \hat{\Theta}_G, \hat{\Theta}_c) \quad (36)$$

$$\hat{\Theta}_G \leftarrow \underset{\Theta_G}{\operatorname{argmax}} \mathcal{L}(\mathcal{D}; \hat{\Theta}_H, \Theta_G, \hat{\Theta}_c) \quad (37)$$

$$\hat{\Theta}_c \leftarrow \underset{\Theta_c}{\operatorname{argmax}} \mathcal{L}(\mathcal{D}; \hat{\Theta}_H, \hat{\Theta}_G, \Theta_c) \quad (38)$$

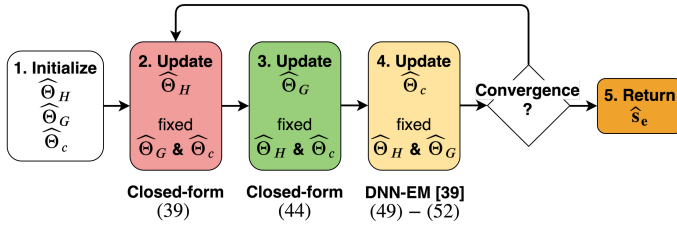


Fig. 4: Flowchart of the proposed BCA algorithm.

The solutions of (36) and (37) are closed-form. As there is no closed-form solution for (38), we propose to use a modified version of Nugraha et al.'s DNN-EM algorithm [39]. The overall flowchart of the proposed algorithm is shown in Fig. 4. Note that it is also possible to optimize the parameters Θ_H , Θ_G and Θ_c with the EM algorithm by adding a nuisance term to (25) [38]. However, this approach would be less efficient to derive the filter parameters Θ_H and Θ_G . In the next subsections, we provide the initialization and the update rules for steps (36)–(38) of our proposed algorithm at iteration i . The derivation of these update rules is detailed in our companion technical report [41].

1) *Initialization* : We initialize the linear filters $\underline{\mathbf{H}}(f)$ and $\underline{\mathbf{G}}(f)$ to $\underline{\mathbf{H}}_0(f)$ and $\underline{\mathbf{G}}_0(f)$, respectively. The PSDs $v_c(n, f)$ of the four sources are jointly initialized using a pretrained DNN denoted as DNN_0 and the SCMs $\mathbf{R}_c(f)$ as the identity matrix \mathbf{I}_M . The inputs, the targets and the architecture of DNN_0 are described in Section IV below.

2) *Echo cancellation filter parameters Θ_H* : The echo cancellation filter $\underline{\mathbf{H}}(f)$ is updated as

$$\underline{\mathbf{h}}(f) = \mathbf{P}(f)^{-1} \mathbf{p}(f), \quad (39)$$

where

$$\mathbf{P}(f) = \sum_{n=0}^{N-1} \underline{\mathbf{X}}_r(n, f)^H \mathbf{R}_{\text{dd}}(n, f)^{-1} \underline{\mathbf{X}}_r(n, f) \quad (40)$$

$$\mathbf{p}(f) = \sum_{n=0}^{N-1} \underline{\mathbf{X}}_r(n, f)^H \mathbf{R}_{\text{dd}}(n, f)^{-1} \mathbf{r}_d(n, f), \quad (41)$$

$\underline{\mathbf{h}}(f) = [\mathbf{h}(0, f)^T \dots \mathbf{h}(K-1, f)^T]^T \in \mathbb{C}^{MK \times 1}$ is a vectorized version of $\underline{\mathbf{H}}(f)$, $\underline{\mathbf{X}}_r(n, f) = [\mathbf{X}_r(n, f) \dots \mathbf{X}_r(n-K+1, f)] \in \mathbb{C}^{M \times MK}$ results from the K taps $\mathbf{X}_r(n-k, f) \in \mathbb{C}^{M \times M}$ obtained by applying the dereverberation filter $\underline{\mathbf{G}}(f)$ on L previous frames of $x(n-k, f)$ as

$$\mathbf{X}_r(n-k, f) = x(n-k, f) \mathbf{I}_M - \sum_{l=\Delta}^{\Delta+L-1} x(n-k-l, f) \mathbf{G}(l, f), \quad (42)$$

and $\mathbf{r}_d(n, f)$ is obtained by applying the dereverberation filter $\underline{\mathbf{G}}(f)$ on $\mathbf{d}(n, f)$ without prior echo cancellation

$$\mathbf{r}_d(n, f) = \mathbf{d}(n, f) - \sum_{k=\Delta}^{\Delta+L-1} \mathbf{G}(k, f) \mathbf{d}(n-k, f) \quad (43)$$

Note that the update of the echo cancellation filter $\underline{\mathbf{H}}(f)$ is influenced by the dereverberation filter $\underline{\mathbf{G}}(f)$ through the terms $\underline{\mathbf{X}}_r(n, f)$ and $\mathbf{r}_d(n, f)$.

3) *Dereverberation filter parameters Θ_G* : Similarly to WPE for dereverberation [30], the dereverberation filter $\underline{\mathbf{G}}(f)$ is updated as

$$\underline{\mathbf{g}}(f) = \mathbf{Q}(f)^{-1} \mathbf{q}(f), \quad (44)$$

where

$$\mathbf{Q}(f) = \sum_{n=0}^{N-1} \underline{\mathbf{E}}(n, f)^H \mathbf{R}_{\text{dd}}(n, f)^{-1} \underline{\mathbf{E}}(n, f), \quad (45)$$

$$\mathbf{q}(f) = \sum_{n=0}^{N-1} \underline{\mathbf{E}}(n, f)^H \mathbf{R}_{\text{dd}}(n, f)^{-1} \mathbf{e}(n, f), \quad (46)$$

$\underline{\mathbf{g}}(f) = [\mathbf{g}_1(\Delta, f)^T \dots \mathbf{g}_M(\Delta, f)^T \dots \mathbf{g}_1(\Delta + L - 1, f)^T \dots \mathbf{g}_M(\Delta + L - 1, f)^T]^T \in \mathbb{C}^{M^2 L \times 1}$ is a vectorized version of $\underline{\mathbf{G}}(f)$, and $\underline{\mathbf{E}}(n, f) = [\mathbf{E}(n-\Delta, f) \dots \mathbf{E}(n-\Delta-L+1, f)] \in \mathbb{C}^{M \times M^2 L}$ results from the L taps $\mathbf{E}(n-l, f) \in \mathbb{C}^{M \times M^2}$ obtained as

$$\mathbf{E}(n-l, f) = \mathbf{I}_M \otimes \mathbf{e}(n-l, f)^T. \quad (47)$$

The update of the dereverberation filter $\underline{\mathbf{G}}(f)$ is influenced by the echo cancellation filter $\underline{\mathbf{H}}(f)$ through the terms $\mathbf{e}(n, f)$.

4) *Variance and spatial covariance parameters Θ_c* : As there is no closed-form solution for the log-likelihood optimization with respect to Θ_c , we estimate the variance and spatial covariance parameters using an EM algorithm. Given the past sequence of the mixture signal $\mathbf{d}(n, f)$, the far-end signal $x(n, f)$ and its past sequence, and the linear filters $\underline{\mathbf{H}}(f)$ and $\underline{\mathbf{G}}(f)$, the residual mixture signal $\mathbf{r}(n, f)$ is conditionally distributed as

$$\mathbf{r}(n, f) \mid \mathbf{d}(n-1, f), \dots, \mathbf{d}(0, f), x(n, f), \dots, x(0, f), \quad (48)$$

$$\underline{\mathbf{H}}(f), \underline{\mathbf{G}}(f) \sim \mathcal{N}_{\mathbb{C}}(\mathbf{0}, \mathbf{R}_{\text{dd}}(n, f)).$$

The signal model is conditionally identical to the local Gaussian modeling framework for source separation [37]. However, this framework does not constraint the PSDs or the SCMs which results in a permutation ambiguity (see Section II-C). Instead, after each update of the linear filters $\underline{\mathbf{H}}(f)$ and $\underline{\mathbf{G}}(f)$, we propose to use one iteration of Nugraha et al.'s DNN-EM algorithm to update the PSDs and the SCMs of the target and residual signals $s_c(n, f)$, $s_r(n, f)$, $\mathbf{z}_r(n, f)$ and $\mathbf{b}_r(n, f)$ [39]. In the E-step, each of these four sources $\mathbf{c}(n, f)$ is estimated as

$$\hat{\mathbf{c}}(n, f) = \mathbf{W}_c(n, f) \mathbf{r}(n, f), \quad (49)$$

and its second-order posterior moment $\hat{\mathbf{R}}_c(n, f)$ as

$$\hat{\mathbf{R}}_c(n, f) = \hat{\mathbf{c}}(n, f) \hat{\mathbf{c}}(n, f)^H + (\mathbf{I} - \mathbf{W}_c(n, f)) v_c(n, f) \mathbf{R}_c(f). \quad (50)$$

In the M-step, the PSDs $v_c(n, f)$ of the four sources are jointly updated using a pretrained DNN denoted as DNN_i , with $i \geq 1$ the iteration index. The inputs, the targets and the architecture of DNN_i are described in Section IV below. For the SCMs $\mathbf{R}_c(f)$, we consider a weighted form of update [42]

$$\mathbf{R}_c(f) = \left(\sum_{n=0}^{N-1} w_c(n, f) \right)^{-1} \sum_{n=0}^{N-1} \frac{w_c(n, f)}{v_c(n, f)} \hat{\mathbf{R}}_c(n, f), \quad (51)$$

where $w_c(n, f)$ denotes the weight of the source $\mathbf{c}(n, f)$. When $w_c(n, f) = 1$, (51) reduces to the exact EM algorithm [37]. Here, we use $w_c(n, f) = v_c(n, f)$ [42], [43]. Experience shows that this weighting trick mitigates inaccurate estimates in certain time-frequency bins and increases the importance of the bins for which $v_c(n, f)$ is large. As the PSDs are constrained, we also need to constrain $\mathbf{R}_c(f)$ so as to encode only the spatial information of the sources. We modify (51) by normalizing $\mathbf{R}_c(f)$ after each update [42]:

$$\mathbf{R}_c(f) \leftarrow \frac{M}{\text{tr}(\mathbf{R}_c(f))} \mathbf{R}_c(f). \quad (52)$$

5) *Estimation of the final early near-end component* $\mathbf{s}_e(n, f)$: Once the proposed iterative optimization algorithm has converged after I iterations, we have estimates of the PSDs $v_c(n, f)$ and the SCMs $\mathbf{R}_c(f)$ and we can ultimately derive the filters $\mathbf{H}(f)$, $\mathbf{G}(f)$ and $\mathbf{W}_{s_e}(n, f)$ to obtain the target estimate $\hat{\mathbf{s}}_e(n, f)$ using (23), (24) and (49). For the detailed pseudo-code of the algorithm, please refer to the supporting document [41].

IV. DNN SPECTRAL MODEL

In this section, we define the inputs, the targets and the architecture of the DNN used to initialize and update the target and residual PSDs.

A. Targets

Estimating $\sqrt{v_c(n, f)}$ has been shown to provide better results than estimating the power spectra $v_c(n, f)$, as the square root compresses the signal dynamics [39]. Therefore we define $\left[\sqrt{v_{s_e}(n, f)} \sqrt{v_{s_r}(n, f)} \sqrt{v_{z_r}(n, f)} \sqrt{v_{b_r}(n, f)} \right]$ as the targets for the DNN. Nugraha et al. defined the ground truth PSDs as $v_c(n, f) = \frac{1}{M} \|\mathbf{c}(n, f)\|^2$ [39]. We thus need to know the ground truth source signals $\mathbf{c}(n, f)$. The ground truth latent signals $\mathbf{s}_r(n, f)$, $\mathbf{z}_r(n, f)$ and $\mathbf{b}_r(n, f)$ are unknown. However, in the training and validation sets, we can know the ground truth early near-end signal $\mathbf{s}_e(n, f)$ and the signals $\mathbf{s}_l(n, f)$, $\mathbf{y}(n, f)$ and $\mathbf{b}(n, f)$ (see Section V-B). These last three signals correspond to the values of $\mathbf{s}_r(n, f)$, $\mathbf{z}_r(n, f)$ and $\mathbf{b}_r(n, f)$, respectively, when the linear filters $\mathbf{H}(f)$ and $\mathbf{G}(f)$ are equal to zero. To derive the ground truth latent signals $\mathbf{s}_r(n, f)$, $\mathbf{z}_r(n, f)$ and $\mathbf{b}_r(n, f)$, we thus propose to use an iterative algorithm similar to the BCA algorithm (see Fig. 4), where the linear filters $\mathbf{H}(f)$ and $\mathbf{G}(f)$ are initialized to zero. At each iteration, we derive the linear filters $\mathbf{H}(f)$ and $\mathbf{G}(f)$ as in (39) and (44), respectively. Instead of using DNN-EM, we update $\mathbf{s}_r(n, f)$, $\mathbf{z}_r(n, f)$ and $\mathbf{b}_r(n, f)$ by applying the linear filters $\mathbf{H}(f)$ and $\mathbf{G}(f)$ to each of the signals $\mathbf{s}_l(n, f)$, $\mathbf{y}(n, f)$ and $\mathbf{b}(n, f)$ as in (26), (27) and (28). For the detailed pseudo-code of this algorithm, please refer to the supporting document [41]. After a few iterations, we observed the convergence of the latent variables $\mathbf{s}_r(n, f)$, $\mathbf{z}_r(n, f)$ and $\mathbf{b}_r(n, f)$. Fig. 5 shows an example of the PSD spectrograms after convergence.

B. Inputs

We use magnitude spectra as inputs for DNN_0 and DNN_i rather than power spectra, since they have been shown to

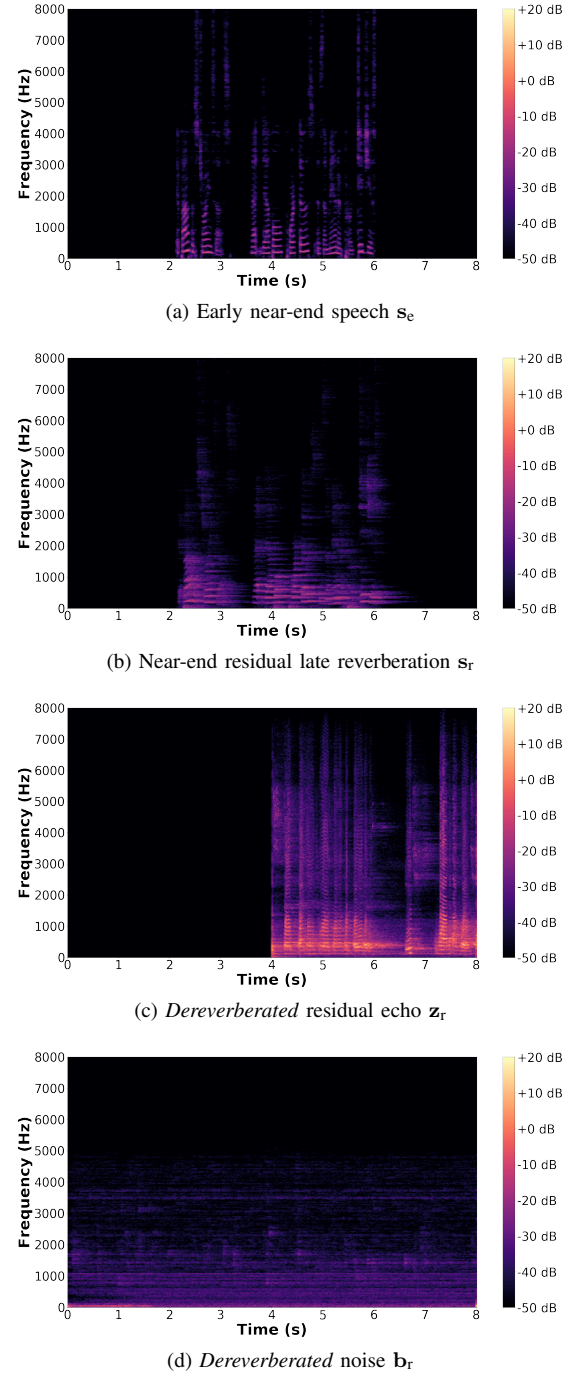


Fig. 5: Example ground truth target and residual signal PSDs in the training set.

provide better results when the targets are the magnitude spectra $\sqrt{v_c(n, f)}$ [39]. We concatenate these spectra to obtain the inputs. The different inputs are summarized in Fig. 6. We consider first the far-end signal magnitude $|x(n, f)|$ and a single-channel signal magnitude $|\tilde{d}(n, f)|$ obtained from the corresponding multichannel mixture signal $\mathbf{d}(n, f)$ as [42]

$$|\tilde{d}(n, f)| = \sqrt{\frac{1}{M} \|\mathbf{d}(n, f)\|^2}. \quad (53)$$

Additionally we use the magnitude spectra $|\tilde{y}(n, f)|$, $|\tilde{e}(n, f)|$, $|\tilde{c}_1(n, f)|$ and $|\tilde{r}(n, f)|$ obtained from the corresponding multi-

channel signals after each linear filtering step $\hat{\mathbf{y}}(n, f)$, $\mathbf{e}(n, f)$, $\hat{\mathbf{e}}_i(n, f)$, $\mathbf{r}(n, f)$. Indeed in our previous work on single-channel echo reduction, using the estimated echo magnitude as an additional input was shown to improve the estimation [26]. We refer to the above inputs as type-I inputs. We consider additional inputs to improve the estimation. In particular, we use the magnitude spectra $\sqrt{v_c^{\text{unc}}(n, f)}$ of the source unconstrained PSDs obtained as

$$v_c^{\text{unc}}(n, f) = \frac{1}{M} \text{tr} \left(\mathbf{R}_c(f)^{-1} \hat{\mathbf{R}}_c(n, f) \right). \quad (54)$$

Indeed these inputs partially contain the spatial information of the sources and have been shown to improve results in source separation [39]. We refer to the inputs obtained from (54) as type-II inputs. For DNN_0 , we only use type-I inputs, as type-II inputs are not available at initialization. For DNN_i with $i \geq 1$, we use both type-I and type-II inputs.

C. Cost function

Let $|\tilde{c}(n, f)|$ denote the DNN output for source $\mathbf{c}(n, f)$. As mentioned above, we use DNN_0 and DNN_i to jointly predict the 4 spectral parameters $\left[|\tilde{s}_e(n, f)| |\tilde{s}_r(n, f)| |\tilde{z}_r(n, f)| |\tilde{b}_r(n, f)| \right]$ (see Fig. 6). We use the Kullback-Leibler divergence as the training loss, which has shown to provide the best results for DNN training among several other losses [39]:

$$\mathcal{D}_{KL} = \frac{1}{4FN} \sum_{c,n,f} \left(\sqrt{v_c(n, f)} \log \frac{\sqrt{v_c(n, f)}}{|\tilde{c}(n, f)|} - \sqrt{v_c(n, f)} + |\tilde{c}(n, f)| \right). \quad (55)$$

D. Architecture

The neural network follows a long-short-term-memory (LSTM) network architecture (see Fig. 6). We consider 1 hidden layer and the number of units for this layer is 1026. The number of inputs is $6F$ for DNN_0 and $10F$ for DNN_i . The activation functions of the hidden layers are rectified linear units (ReLU). Other network architectures are not considered here as the performance comparison between different architectures is beyond the scope of this article.

V. EXPERIMENTAL PROTOCOL

In this section we describe the datasets, the metrics, the baselines and the hyperparameter settings used to evaluate the proposed algorithm.

A. Scenario

We consider the scenario where a near-end speaker interacts with a far-end speaker using a hands-free communication system at a distance of 1.5 m in a noisy environment. Each utterance has 8-s duration and contains 4 s of near-end speech and 4 s of far-end speech overlapping for 2 s. Background noise is present during the whole utterance. Each utterance is hence composed of 4 periods of 2 s as shown in Fig. 7: 1) noise only, 2) noise and near-end speech, 3) noise, near-end and far-end speech, 4) noise and far-end speech.

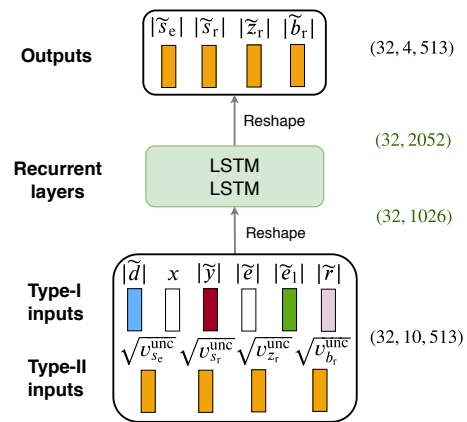


Fig. 6: Architecture of DNN_i with a sequence length of 32 timesteps and $F = 513$ frequency bins.

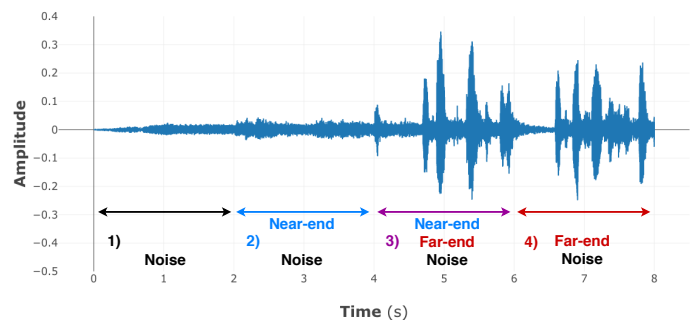


Fig. 7: Example utterance (only one channel shown).

B. Datasets

1) *Overall description:* We created three disjoint datasets for training, validation and test, whose characteristics are summarized in Table I. We considered $M = 3$ microphones. For each dataset, we separately recorded or simulated the acoustic echo $\mathbf{y}(t)$, the near-end speech $\mathbf{s}(t)$ and the noise $\mathbf{b}(t)$ using clean speech and noise signals as base material and we computed the mixture signal $\mathbf{d}(t)$ as in (15). This protocol is required to obtain the ground truth target and residual signals for training and evaluation, which is not possible with real-world recordings for which these ground truth signals are unknown. The training and validation sets correspond to time-invariant acoustic conditions, while the test set includes both a time-invariant and a time-varying subset. The recording and simulation parameters are detailed in our companion technical report [41].

a) *Clean speech and noise signals:* Clean speech signals were taken from the train-clean-360 subset of the Librispeech corpus [44], which consists of 921 speakers reading books for 25 min each on average. We selected 262 speakers and grouped them into 131 disjoint pairs for training, validation, and test. We alternately considered each speaker as near-end or far-end and picked several non-overlapping 4-s speech samples for each pair. Each 4-s sample was used only once in the whole dataset. Regarding the noise signals, we considered 6 types of domestic noise: babble, dishwasher, fridge, microwave, vacuum cleaner and washing machine. We randomly selected

| Dataset | Training | Validation | Test |
|-----------------|-------------------|--|--------------|
| Signals | y s b | recorded simulated a_s simulated | recorded |
| Rooms | 1-2-3 | 1-2 | 4 |
| # speaker pairs | 79 | 27 | 25 |
| # utterances | 13,572 | 4,536 | 4,500 |
| # noise samples | 36 | 36 | 6 |
| SER range (dB) | | $[-45, +6]$ | $[-45, -7]$ |
| SNR range (dB) | | $[-21, +24]$ | $[-20, +13]$ |

TABLE I: Dataset characteristics.

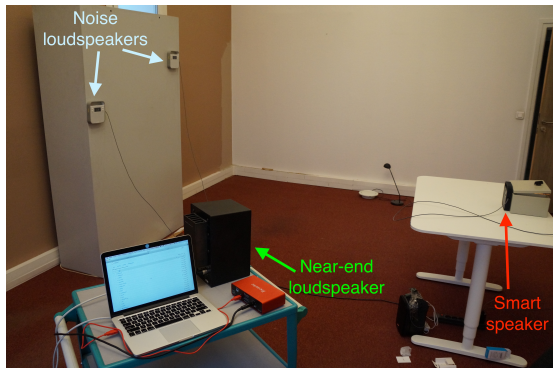


Fig. 8: Recording setup for the test set.

78 non-overlapping 8-s noise samples from 1.7 h of YouTube videos and grouped them into disjoint subsets for training, validation, and test.

b) Real echo recordings: To create the acoustic echo $y(t)$, Togami et al. convolved far-end speech signals $x(t)$ with simulated echo paths $a_y(\tau)$ which do not include any nonlinearity [19]. In real hands-free systems, the acoustic echo contains nonlinearities caused by the nonlinear response of the loudspeaker, enclosure vibrations and hard clipping effects due to amplification (see Section II-A). In order to achieve more realistic test conditions, we created the acoustic echo by recording the acoustic feedback from the loudspeaker to the microphones of a real hands-free system. The far-end speech was played and recorded at a rate of 16 kHz with a Tribby, a smart speaker device developed by Invoxia. A configuration of the echo recording setup is given in Fig. 8. The recordings were done with the same Tribby in 4 rooms with different size and reverberation time (RT_{60}) listed in Table II.

c) Reverberant near-end speech and noise: The creation procedures for $s(t)$ and $b(t)$ differ for each dataset and are described in the following subsections.

2) Training set: For the training set, the echo recordings were done in rooms 1, 2 and 3 (see Table II). To create the reverberant near-end speech $s(t)$, we convolved anechoic near-end speech $u(t)$ with near-end RIRs $a_s(\tau)$ simulated to match the echo recording properties using the Roomsimove toolbox [45] [41]. Among the 79 pairs of speakers used for training, 54 were used in rooms 1 and 2. We played and recorded 4,536 far-end signals and we simulated 4,536 near-end RIRs in each of these 2 rooms. The remaining 25 pairs were used in room 3. We played and recorded 4,500 far-end signals and

| Room | Size (m) | RT_{60} (s) |
|------|-----------------------------|---------------|
| 1 | $4.4 \times 4.2 \times 4$ | 1.0 |
| 2 | $3.8 \times 2.5 \times 3.5$ | 0.5 |
| 3 | $3.4 \times 2.1 \times 3.3$ | 0.8 |
| 4 | $3.4 \times 2.1 \times 3.3$ | 1.3 |

TABLE II: Room characteristics.

we simulated 4,500 near-end RIRs in this room. To create the noise signal $b(t)$, we measured 42 RIRs in rooms 1, 2 and 3, and we convolved a randomly chosen noise sample among the 36 noise samples (6 per noise type) used for training with the average of two RIRs randomly picked among the 42 measured RIRs to simulate a spatially diffuse signal. The levels of the recorded far-end, the near-end speech and the noise signal were chosen randomly such that the signal-to-echo ratio (SER) varied from -45 dB to $+6$ dB and the signal-to-noise ratio (SNR) varied from -21 dB to $+24$ dB. These conditions are very challenging, especially as reverberation dominates in the reverberant near-end speech $s(t)$. In total, we obtained 13,572 utterances which amount to roughly 32 h of audio.

3) Validation set: The validation set was generated in a similar way as the training set, using 27 speaker pairs and 36 noise samples that are not in the training set. The echo recordings were done in rooms 1 and 2, and the near-end RIRs were simulated similarly to the training set procedure. We played and recorded 4,536 far-end signals and we simulated 4,536 near-end RIRs in each room. To create the diffuse noise, we used the same 42 measured RIRs as in the training set. The levels of the recorded far-end speech, the near-end speech and the noise signal were chosen in the same range as the training set, resulting in the same challenging SER and SNR conditions. In total, we obtained 4,536 utterances which amount to roughly 10 h of audio.

4) Time-invariant test set: The time-invariant test set was built from real recordings only, using 25 speaker pairs and 6 noise samples that are neither in the training nor in the validation sets. The echo, the near-end speech and the noise were all recorded in room 4 (see Table II) using the setup shown in Fig. 8. The reverberant near-end speech $s(t)$ was obtained by playing anechoic speech with a Yamaha MSP5 Studio loudspeaker at a single loudness level. The noise signal $b(t)$ was obtained by picking a random original noise signal and playing it through 4 Tribby loudspeakers simultaneously. The noise signals resulting from this procedure are less diffuse than in the training and validation sets. The recorded levels were such that the resulting SER varied from -45 dB to -7 dB and the SNR varied from -20 dB to $+13$ dB. These challenging conditions are comprised within those of the training and validation sets. We played and recorded 4,500 far-end speech, near-end speech, and noise signals, hence we obtained a total of 4,500 8-s utterances amounting to 7.5 h of audio.

5) Time-varying test set: In order to evaluate our approach in time-varying acoustic conditions, we also considered the scenario when the near-end speaker speaks for 4 s, moves to a different position, and speaks for 4 s again. To do so, we

| | |
|--------|--|
| ERLE | $10 \log_{10} \frac{\ y\ ^2}{\ z_r^{\text{post}}\ ^2}$ |
| SER | $10 \log_{10} \frac{\ s_e^{\text{post}}\ ^2}{\ z_r^{\text{post}}\ ^2}$ |
| ELR | $10 \log_{10} \frac{\ s_e^{\text{post}}\ ^2}{\ s_f^{\text{post}}\ ^2}$ |
| SNR | $10 \log_{10} \frac{\ s_e^{\text{post}}\ ^2}{\ b_r^{\text{post}}\ ^2}$ |
| SI-SAR | $10 \log_{10} \frac{\ \alpha s_e\ ^2}{\ \alpha s_e - s_e^{\text{post}}\ ^2}$ |
| SI-SDR | $10 \log_{10} \frac{\ \alpha s_e\ ^2}{\ \alpha s_e - \hat{s}_e\ ^2}$ |

TABLE III: Evaluation metrics. The formulas are given in the single-channel case and the channel index is omitted for conciseness.

concatenated pairs of 8-s near-end and echo recordings from the time-invariant test set corresponding to the same near-end and far-end speakers and microphone array positions, but to two different positions of the loudspeaker playing the near-end speech. The two recordings summed with an 16 s recorded noise signal. This resulted in 2,250 16-s utterances or roughly 11 h of audio.

C. Evaluation metrics

The estimated early near-end $\hat{s}_e(n, f)$ has 4 components

$$\hat{s}_e(n, f) = s_e^{\text{post}}(n, f) + s_r^{\text{post}}(n, f) + z_r^{\text{post}}(n, f) + b_r^{\text{post}}(n, f), \quad (56)$$

where $s_e^{\text{post}}(n, f)$ is the potentially distorted early near-end signal, and $s_r^{\text{post}}(n, f)$, $z_r^{\text{post}}(n, f)$ and $b_r^{\text{post}}(n, f)$ are the post-residual distortion sources that are ideally equal to zero vectors. The objective metrics used to assess the reduction of each distortion source are summarized in Table III. They are computed separately for each channel and averaged over the channels. Since the performance may vary depending on the presence of acoustic echo which is the loudest signal, we compute the metrics separately for *near-end talk* (near-end speech only), *double-talk* (simultaneous near-end and far-end speech) and *far-end talk* (far-end speech only) and average them in the fashion of the segmental SNR [46]. For echo reduction, we use the SER and the echo return loss enhancement (ERLE) [3]. The SER is only evaluated during *double-talk*, while the ERLE is evaluated during both *far-end talk* and *double-talk*. Dereverberation is assessed by the early-to-late reverberation ratio (ELR) [2]. We use this metric instead of the direct-to-reverberant ratio (DRR) [2] since early reflections are part of the target signal to be estimated. For noise reduction, we use the SNR. The near-end speech distortion is measured with the scale-invariant signal-to-artifacts ratio (SI-SAR) and the overall distortion with the scale-invariant signal-to-distortion ratio (SI-SDR) [47]. The latter two metrics rely on the estimation of a scaling factor α , which is assumed to be constant during each *near-end talk*, *double-talk* or *far-end talk* period, but may vary from one period to another.

All the above metrics are based on the energy of the post-residual distortion signals defined in (56). These signals can be computed by applying the estimated echo cancellation filter,

dereverberation filter and Wiener postfilter to the target $s_e(t)$ and the ground truth late reverberation $s_l(t)$, echo $y(t)$ and noise $b(t)$ signals separately. The dataset generation procedure readily provides ground truth signals for the echo and the noise. To define the target and ground truth late reverberation signals, we set the mixing time as $t_e = 0.064$ ms. We computed these two components using (8). In the test set, since the ground truth near-end RIR $a_s(\tau)$ is unknown, we used the method proposed by Yoshioka et al. instead, which estimates $a_s(\tau)$ by MMSE optimization between the reverberant near-end speech $s(t)$ and the anechoic near-end speech $u(t)$ [8], [30].

D. Baselines

We compare our offline approach with two baselines: 1) our implementation of Togami et al.'s approach [19] and 2) a cascade approach where the echo cancellation filter $\underline{\mathbf{H}}(f)$, the dereverberation filter $\underline{\mathbf{G}}(f)$ and the Wiener postfilter $\underline{\mathbf{W}}_{s_e}(n, f)$ are estimated and applied one after another. Echo cancellation relies on SpeexDSP¹, which implements Valin's adaptive approach and is particularly suitable for time-varying conditions [48] (see Section II-A). Dereverberation relies on our implementation of WPE [29], [30] (see Section II-B). The multichannel Wiener postfilter is computed using our implementation of Nugraha et al.'s DNN-EM approach [39] (see Section II-C).

E. Hyperparameter settings

The hyperparameters of the three approaches are set as follows.

1) *Initialization of the linear filters*: For echo cancellation, we compute $\underline{\mathbf{H}}_0(f)$ by applying SpeexDSP on each channel of $d(n, f)$. Since SpeexDSP relies on half-overlapping rectangular STFT windows, we use a window of length 512 and hopsize 256. We set the filter length to 0.208 s in the time domain, that is $K = 13$ frames. As SpeexDSP is an online algorithm, we apply it twice to each utterance to ensure convergence. For dereverberation, we compute $\underline{\mathbf{G}}_0(f)$ by performing 3 iterations of WPE on the signal $e(t)$ output by SpeexDSP. We use the STFT with a Hanning window of length 1,024 and hopsize 256. We set the filter length to 0.208 s in the time domain, that is $L = 10$ frames, and the delay to $\Delta = 3$ frames.

2) *Hyperparameters of the DNN-based BCA algorithm*: The STFT coefficients are computed with a Hanning window of length 1,024 and hopsize 256 resulting in $F = 513$ frequency bins. The length of the echo cancellation filter $\underline{\mathbf{H}}(f)$ (0.208 s in the time domain) now corresponds to $K = 10$ frames. The hyperparameters of the dereverberation filter $\underline{\mathbf{G}}(f)$ are identical to those of WPE. At training time, we perform 3 iterations of the iterative procedure to derive the ground truth PSDs (see Section IV-A) [41]. DNN training is done by backpropagation with a minibatch size of 16 sequences, a fixed sequence length of 32 frames and the Adam parameter update algorithm with default settings [49]. To

¹<https://github.com/xiph/speexdsp>

avoid gradient explosion with long sequences, we use gradient clipping with a threshold of 1.0. Training is stopped when the loss on the validation set stops decreasing for 5 epochs. At test time, we perform $I = 2$ iterations of the proposed DNN-based BCA algorithm [41] with 1 spatial and 1 spectral update for each iteration i [42] (see Fig. 4).

3) *Hyperparameters of Togami et al.'s joint approach [19]:* Togami et al.'s approach requires the initial values for the linear filters $\underline{\mathbf{H}}(f)$ and $\underline{\mathbf{G}}(f)$, and for the PSDs of the reverberant near-end speech $v_s(n, f) = \frac{1}{M} \|\mathbf{s}(n, f)\|^2$ and the noise signal $v_b(n, f) = \frac{1}{M} \|\mathbf{b}(n, f)\|^2$. We initialize $\underline{\mathbf{H}}(f)$ and $\underline{\mathbf{G}}(f)$ by applying SpeexDSP and WPE on $\mathbf{d}(n, f)$, respectively, with the same hyperparameters as above. Since the authors did not specify how to initialize the PSDs [19], we estimate them using a DNN similar to DNN_0 where the type-I input for $|\tilde{e}_1(n, f)|$ is replaced by $|\tilde{d}_1(n, f)|$ obtained similarly to (53) from the corresponding multichannel signal $\hat{\mathbf{d}}_1(n, f) = \sum_{l=\Delta}^{\Delta+L-1} \mathbf{G}(l, f) \mathbf{d}(n-l, f)$ (see Fig. 2). All the SCMs are initialized to \mathbf{I}_M . We perform 3 iterations of Togami et al.'s EM algorithm using the same STFT hyperparameters and values of K , L and Δ as for our approach.

4) *Hyperparameters of the cascade approach:* We compute and fix the linear filters to $\underline{\mathbf{H}}(f) = \underline{\mathbf{H}}_0(f)$ and $\underline{\mathbf{G}}(f) = \underline{\mathbf{G}}_0(f)$ with the same hyperparameters as the proposed approach. Using $\underline{\mathbf{H}}_0(f)$ for echo cancellation is particularly efficient in time-varying conditions (see Section II-A). The DNN architecture and inputs are identical to those in our approach, and the ground truth PSDs are computed using the same procedure where the linear filters are fixed to $\underline{\mathbf{H}}(f) = \underline{\mathbf{H}}_0(f)$ and $\underline{\mathbf{G}}(f) = \underline{\mathbf{G}}_0(f)$ (see Section IV-A). Note that the type-I inputs for $|\tilde{y}(n, f)|$, $|\tilde{e}(n, f)|$, $|\tilde{e}_1(n, f)|$ and $|\tilde{r}(n, f)|$ remain fixed over the EM iterations because of the fixed linear filters.

5) *Regularization:* In order to avoid numerical instabilities and ill-conditioned matrices, we add a regularization scalar ϵ to the denominator in (51) and a regularization matrix $\epsilon \mathbf{I}$ to the matrix to be inverted in (31), (39) and (44). We also regularize the training loss in (55) similarly to Nugraha et al. [39]. We regularize likewise Togami et al.'s joint approach and the cascade approach. The regularization hyperparameter is fixed to $\epsilon = 10^{-5}$.

VI. RESULTS AND DISCUSSION

In this section, our proposed approach for joint reduction of echo, reverberation and noise is compared Togami et al.'s approach and the cascade approach. First we analyze the results of the three approaches in time-invariant conditions. Finally we discuss their results in time-varying conditions and we compare their computation time. Audio examples are provided online².

A. Time-invariant conditions

1) *Average performance:* Fig. 9a shows the average results in time-invariant conditions. All approaches have a negative SI-SDR, which is caused by the challenging test set conditions. The proposed approach outperforms the cascade approach in

terms of SI-SDR by 1 dB. While the performance in terms of ELR is comparable between the 2 approaches, the performance in terms of SI-SDR is justified by the better performance of the proposed approach in terms of SER, SNR, SI-SAR and ERLE. The difference is particularly significant in terms of SER, which is induced by greater ERLE (greater echo reduction) and greater SI-SAR (lower degradation of the target \mathbf{s}_e).

The proposed approach also outperforms Togami et al.'s approach in terms of SI-SDR by 4 dB. Although their approach has comparable SER and significantly greater ELR and SNR, the difference in terms of SI-SDR is explained by significantly lower SI-SAR (9 dB difference), which is additionally negative (close to -3 dB). This means that their approach significantly degrades the target \mathbf{s}_e compared to the proposed approach. This degradation is partly caused by the application in parallel of the linear filters $\underline{\mathbf{H}}(f)$ and $\underline{\mathbf{G}}(f)$ (see Section II-D). Indeed we found that the *dereverberated* residual echo \mathbf{z}_r in the signal \mathbf{r} is systematically higher with their approach than with the proposed and cascade approaches. Although their approach provides much greater ERLE, this degradation mitigates their performance in SER.

2) *Interactions of system components:* While the above results show the performance averaged over all periods (*near-end talk*, *far-end talk* and *double-talk*), we need further performance analysis when only echo and reverberation are present, i.e. during *near-end talk*, and when echo, reverberation and noise are present simultaneously, i.e. during *double-talk*, to investigate how the system components interact with each other. We discard the analysis of *far-end talk* as the target \mathbf{s}_e is absent in this scenario.

Fig. 10a shows the results during *near-end talk*. SER and ERLE are not evaluated as echo is absent. All approaches have a SI-SDR that is positive or close to 0 dB. The proposed approach performs similarly or slightly better than the cascade approach for all metrics. Thus joint optimization does not improve performance during *near-end talk*, but does not degrade it either. Togami et al.'s approach outperforms the proposed approach in terms of ELR and SNR, but is outperformed in terms of SI-SDR, which is due to the great SI-SAR difference.

Fig. 10b shows the results during *double-talk*. The trend in performance between the approaches is similar to the results averaged over all periods. However, the proposed approach has greater difference in terms of SI-SDR due greater SI-SAR difference, i.e. lower degradation of the target \mathbf{s}_e during *double-talk*.

Between *near-end talk* to *double-talk*, SI-SDR decreases by 4.7 dB for the proposed approach, by 6.3 dB for the cascade approach and by 8.9 dB for Togami et al.'s approach. We conclude that the proposed joint optimization improves robustness in terms of SI-SDR and SI-SAR when echo, reverberation and noise are present simultaneously, while not degrading performance when only reverberation and noise are present.

B. Time-varying conditions

Fig. 9b shows the average results in time-varying conditions. The SI-SDR decreases for all approaches since the spatial

²<https://team.inria.fr/multispeech/demos>

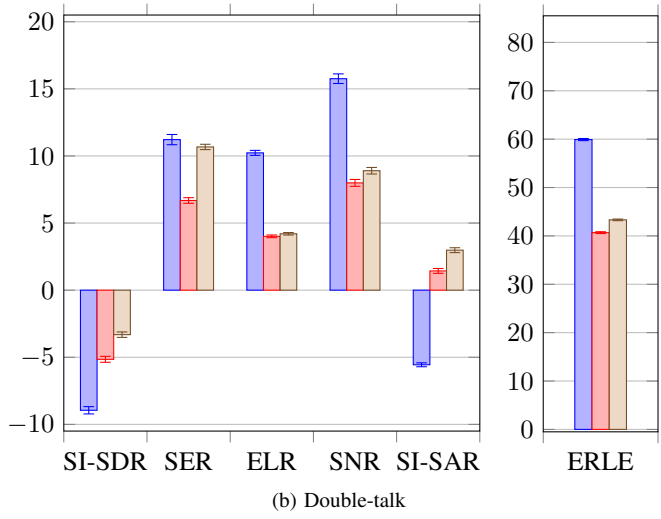
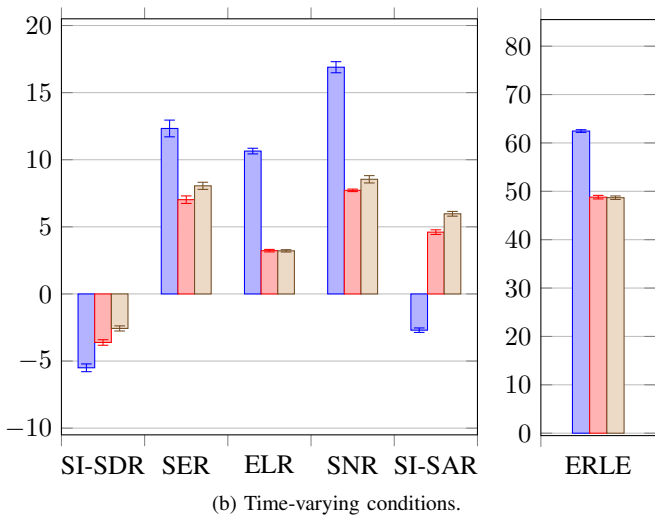
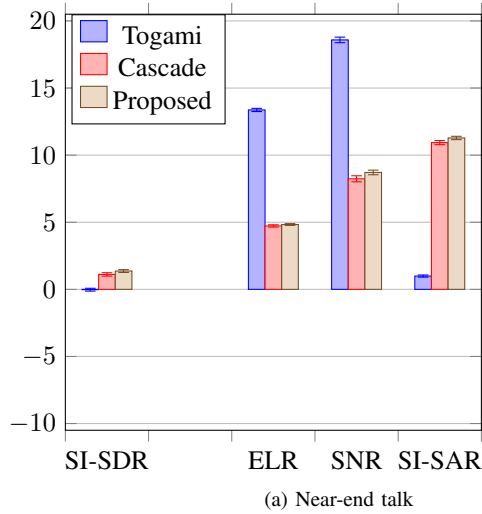
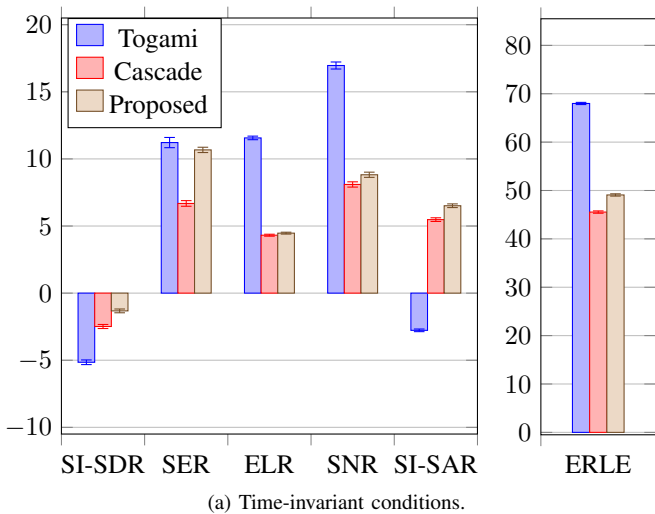


Fig. 9: Average results.

Fig. 10: Analysis in time-invariant conditions.

properties of target s_e and the near-end residual reverberation s_r vary over time while their SCMs remain fixed. However the trend in performance is similar to the average performance in time-invariant conditions. Although the proposed approach is not designed for time-varying conditions, it still outperforms the 2 others approaches in terms of SI-SDR. Additionally, it still outperforms the cascade approach in terms of SER, even though the cascade approach uses Valin’s adaptive approach for echo cancellation which is designed for time-varying conditions [48] (see Section II-A).

C. Computation time

We discard the initialization as it is the same for all 3 approaches (see Section V-E). With a 2.7 GHz Intel Core i5 CPU, computing the target \hat{s}_e for a 8 s utterance took 12% more time for the proposed approach and 43% less time for Togami et al.’s approach compared to the cascade approach. Since the cascade approach is one of the approaches implemented in today’s industrial devices, we conclude that the proposed approach can be implemented in real time.

VII. CONCLUSION

We proposed a DNN-based BCA algorithm for joint multichannel reduction of acoustic echo, reverberation and noise. The approach jointly models the spectra of the target and residual signals after echo cancellation and dereverberation with a DNN. We evaluated our system on real recordings of acoustic echo, reverberation and noise acquired with a smart speaker in various situations. When echo, reverberation and noise are present simultaneously, the proposed approach outperforms the cascade approach and Togami et al.’s joint reduction approach in terms of overall distortion reduction while not degrading performance when only reverberation and noise are present. Future work will focus on a recursive version of the approach in order to better handle time-varying conditions.

REFERENCES

- [1] E. Vincent, T. Virtanen, and S. Gannot, *Audio Source Separation and Speech Enhancement*. Wiley, 2018.
- [2] P. A. Naylor and N. D. Gaubitch, Eds., *Speech Dereverberation*. Springer, 2010.
- [3] E. Hansler and G. Schmidt, *Acoustic Echo and Noise Control: a Practical Approach*. Wiley-Interscience, 2004.

- [4] J. S. Erkelens and R. Heusdens, "Correlation-based and model-based blind single-channel late-reverberation suppression in noisy time-varying acoustical environments," *IEEE Transactions on Audio, Speech, and Language Processing*, vol. 18, no. 7, pp. 1746–1765, 2010.
- [5] I. Kodrasi and S. Doclo, "Joint dereverberation and noise reduction based on acoustic multi-channel equalization," *IEEE/ACM Transactions on Audio, Speech, and Language Processing*, vol. 24, no. 4, pp. 680–693, 2016.
- [6] O. Schwartz, S. Gannot, and E. A. P. Habets, "Multi-microphone speech dereverberation and noise reduction using relative early transfer functions," *IEEE/ACM Transactions on Audio, Speech, and Language Processing*, vol. 23, no. 2, pp. 240–251, 2015.
- [7] T. Dietzen, S. Doclo, M. Moonen, and T. van Waterschoot, "Joint multi-microphone speech dereverberation and noise reduction using integrated sidelobe cancellation and linear prediction," in *Proc. IWAENC*, 2018, pp. 221–225.
- [8] T. Yoshioka, T. Nakatani, M. Miyoshi, and H. G. Okuno, "Blind separation and dereverberation of speech mixtures by joint optimization," *IEEE Transactions on Audio, Speech, and Language Processing*, vol. 19, no. 1, pp. 69–84, 2011.
- [9] H. Kagami, H. Kameoka, and M. Yukawa, "Joint separation and dereverberation of reverberant mixtures with determined multichannel non-negative matrix factorization," in *Proc. ICASSP*, 2018, pp. 31–35.
- [10] R. Le Bouquin Jeannès, P. Scalart, G. Faucon, and C. Beauguant, "Combined noise and echo reduction in hands-free systems: a survey," *IEEE Transactions on Speech and Audio Processing*, vol. 9, no. 8, pp. 808–820, 2001.
- [11] S. Gustafsson, R. Martin, P. Jax, and P. Vary, "A psychoacoustic approach to combined acoustic echo cancellation and noise reduction," *IEEE Transactions on Speech and Audio Processing*, vol. 10, no. 5, pp. 245–256, 2002.
- [12] W. Herbordt, S. Nakamura, and W. Kellermann, "Joint optimization of LCMV beamforming and acoustic echo cancellation for automatic speech recognition," in *Proc. ICASSP*, 2005, pp. III–77–80.
- [13] G. Reuven, S. Gannot, and I. Cohen, "Joint noise reduction and acoustic echo cancellation using the transfer-function generalized sidelobe canceller," *Speech Communication*, vol. 49, no. 7–8, pp. 623–635, 2007.
- [14] M. Togami, Y. Kawaguchi, and R. Takashima, "Frequency domain acoustic echo reduction based on Kalman smoother with time-varying noise covariance matrix," in *Proc. ICASSP*, 2014, pp. 5909–5913.
- [15] K. Nathwani, "Joint acoustic echo and noise cancellation using spectral domain Kalman filtering in double talk scenario," in *Proc. IWAENC*, 2018, pp. 326–330.
- [16] R. Takeda, K. Nakadai, T. Takahashi, K. Komatani, T. Ogata, and H. G. Okuno, "ICA-based efficient blind dereverberation and echo cancellation method for barge-in-able robot audition," in *Proc. ICASSP*, 2009, pp. 3677–3680.
- [17] M. Togami and Y. Kawaguchi, "Speech enhancement combined with dereverberation and acoustic echo reduction for time varying systems," in *Proc. SSP*, 2012, pp. 357–360.
- [18] E. A. P. Habets, S. Gannot, I. Cohen, and P. C. Sommen, "Joint dereverberation and residual echo suppression of speech signals in noisy environments," *IEEE Transactions on Audio, Speech, and Language Processing*, vol. 16, no. 8, pp. 1433–1451, 2008.
- [19] M. Togami and Y. Kawaguchi, "Simultaneous optimization of acoustic echo reduction, speech dereverberation, and noise reduction against mutual interference," *IEEE/ACM Transactions on Audio, Speech, and Language Processing*, vol. 22, no. 11, pp. 1612–1623, 2014.
- [20] D. S. Williamson and D. Wang, "Speech dereverberation and denoising using complex ratio masks," in *Proc. ICASSP*, 2017, pp. 5590–5594.
- [21] Y. Zhao, Z.-Q. Wang, and D. Wang, "A two-stage algorithm for noisy and reverberant speech enhancement," in *Proc. ICASSP*, 2017, pp. 5580–5584.
- [22] H. Seo, M. Lee, and J.-H. Chang, "Integrated acoustic echo and background noise suppression based on stacked deep neural networks," *Applied Acoustics*, vol. 133, pp. 194–201, 2018.
- [23] H. Zhang and D. Wang, "Deep learning for acoustic echo cancellation in noisy and double-talk scenarios," in *Interspeech*, 2018, pp. 3239–3243.
- [24] F. Yang, G. Enzner, and J. Yang, "Statistical convergence analysis for optimal control of DFT-domain adaptive echo canceler," *IEEE/ACM Transactions on Audio, Speech, and Language Processing*, vol. 25, no. 5, pp. 1095–1106, 2017.
- [25] C. M. Lee, J. W. Shin, and N. S. Kim, "DNN-based residual echo suppression," in *Interspeech*, 2015, pp. 316–320.
- [26] G. Carbajal, R. Serizel, E. Vincent, and E. Humbert, "Multiple-input neural network-based residual echo suppression," in *Proc. ICASSP*, 2018, pp. 231–235.
- [27] G. Enzner and P. Vary, "Frequency-domain adaptive Kalman filter for acoustic echo control in hands-free telephones," *Signal Processing*, vol. 86, no. 6, pp. 1140–1156, 2006.
- [28] M. Togami and K. Hori, "Multichannel semi-blind source separation via local Gaussian modeling for acoustic echo reduction," in *Proc. EUSIPCO*, 2011, pp. 496–500.
- [29] T. Nakatani, T. Yoshioka, K. Kinoshita, M. Miyoshi, and B. H. Juang, "Speech dereverberation based on variance-normalized delayed linear prediction," *IEEE Transactions on Audio, Speech, and Language Processing*, vol. 18, no. 7, pp. 1717–1731, 2010.
- [30] T. Yoshioka and T. Nakatani, "Generalization of multi-channel linear prediction methods for blind MIMO impulse response shortening," *IEEE Transactions on Audio, Speech, and Language Processing*, vol. 20, no. 10, pp. 2707–2720, 2012.
- [31] A. Jukic, T. van Waterschoot, T. Gerkmann, and S. Doclo, "Multi-Channel Linear Prediction-Based Speech Dereverberation With Sparse Priors," *IEEE/ACM Transactions on Audio, Speech, and Language Processing*, vol. 23, no. 9, pp. 1509–1520, 2015.
- [32] K. Kinoshita, M. Delcroix, H. Kwon, T. Mori, and T. Nakatani, "Neural network-based spectrum estimation for online WPE dereverberation," in *Interspeech*, 2017, pp. 384–388.
- [33] K. Furuja and A. Kataoka, "Robust speech dereverberation using multichannel blind deconvolution with spectral subtraction," *IEEE Transactions on Audio, Speech and Language Processing*, vol. 15, no. 5, pp. 1579–1591, 2007.
- [34] M. Togami, Y. Kawaguchi, R. Takeda, Y. Obuchi, and N. Nukaga, "Optimized speech dereverberation from probabilistic perspective for time varying acoustic transfer function," *IEEE Transactions on Audio, Speech, and Language Processing*, vol. 21, no. 7, pp. 1369–1380, 2013.
- [35] A. Cohen, G. Stemmer, S. Ingalsuo, and S. Markovich-Golan, "Combined weighted prediction error and minimum variance distortionless response for dereverberation," in *Proc. ICASSP*, 2017, pp. 446–450.
- [36] S. Gannot, E. Vincent, S. Markovich-Golan, and A. Ozerov, "A consolidated perspective on multimicrophone speech enhancement and source separation," *IEEE/ACM Transactions on Audio, Speech, and Language Processing*, vol. 25, no. 4, pp. 692–730, 2017.
- [37] N. Q. K. Duong, E. Vincent, and R. Gribonval, "Under-determined reverberant audio source separation using a full-rank spatial covariance model," *IEEE Transactions on Audio, Speech, and Language Processing*, vol. 18, no. 7, pp. 1830–1840, 2010.
- [38] A. Ozerov and C. Févotte, "Multichannel nonnegative matrix factorization in convolutive mixtures for audio source separation," *IEEE Transactions on Audio, Speech, and Language Processing*, vol. 18, no. 3, pp. 550–563, 2010.
- [39] A. A. Nugraha, A. Liutkus, and E. Vincent, "Multichannel audio source separation with deep neural networks," *IEEE/ACM Transactions on Audio, Speech, and Language Processing*, vol. 24, no. 9, pp. 1652–1664, 2016.
- [40] S. Leglaive, L. Girin, and R. Horaud, "Semi-supervised multichannel speech enhancement with variational autoencoders and non-negative matrix factorization," in *Proc. ICASSP*, 2019, pp. 101–105.
- [41] G. Carbajal, R. Serizel, E. Vincent, and E. Humbert, "Joint DNN-based multichannel reduction of echo, reverberation and noise: Supporting document," Inria, Tech. Rep. RR-9284, 2019. [Online]. Available: <https://hal.inria.fr/hal-02372431>
- [42] A. A. Nugraha, A. Liutkus, and E. Vincent, "Multichannel music separation with deep neural networks," in *Proc. EUSIPCO*, 2016, pp. 1748–1752.
- [43] A. Liutkus, D. Fitzgerald, and Z. Rafii, "Scalable audio separation with light kernel additive modelling," in *Proc. ICASSP*, 2015, pp. 76–80.
- [44] V. Panayotov, G. Chen, D. Povey, and S. Khudanpur, "Librispeech: an ASR corpus based on public domain audio books," in *Proc. ICASSP*, 2015, pp. 5206–5210.
- [45] E. Vincent and D. R. Campbell, "Roomsimove," 2008. [Online]. Available: http://homepages.loria.fr/evincent/software/Roomsimove_1.4.zip
- [46] P. C. Loizou, *Speech Enhancement: Theory and Practice*. CRC Press, 2007.
- [47] J. Le Roux, S. Wisdom, H. Erdogan, and J. R. Hershey, "SDR — half-baked or well done?" in *Proc. ICASSP*, 2019, pp. 626–630.
- [48] J. M. Valin, "On adjusting the learning rate in frequency domain echo cancellation with double-talk," *IEEE Transactions on Audio, Speech, and Language Processing*, vol. 15, no. 3, pp. 1030–1034, 2007.
- [49] D. P. Kingma and J. Ba, "Adam: A method for stochastic optimization," in *Proc. ICLR*, 2015.